Hindawi
Journal of Engineering
Volume 2023, Article ID 4031238, 18 pages
https://doi.org/10.1155/2023/4031238

Research Article

Comprehensive Thermal Characteristic Investigations on Hemp- and Jute-Based Nature Fibre-Reinforced Composites for Engineering Applications through Coupled and Verified Engineering Approaches

Sabari Thangavel,[1] **Mohamed Aashik Jaffar Ali**,[1] **Raj Kumar Gnanasekaran**,[1] **Beena Stanislaus Arputharaj**,[2] **Arunkumar Karuppasamy**,[3] **Hussein A. Z. AL-Bonsrulah**,[4,5] **Parvathy Rajendran**,[6] **Vijayanandh Raja**,[1] **Devendhiran Soundararajan**,[1] **and Krishnakumar Kalaivani Muthuramalingam**[7]

[1]*Department of Aeronautical Engineering, Kumaraguru College of Technology, Coimbatore 641049, Tamil Nadu, India*
[2]*Department of Research and Innovation, Saveetha School of Engineering, SIMATS, Chennai 602105, Tamil Nadu, India*
[3]*Department of Aeronautical Engineering, MLR Institute of Technology, Hyderabad, Telangana, India*
[4]*Mechanical Power Technical Engineering Department, Al-Amarah University College, Maysan, Iraq*
[5]*Department of Computer Techniques Engineering, AlSafwa University College, Karbala 56001, Iraq*
[6]*School of Aerospace Engineering, Universiti Sains Malaysia, Engineering Campus, Nibong Tebal 14300, Pulau Pinang, Malaysia*
[7]*Aircraft Design Engineering, National Aerospace University-Kharkiv Aviation Institute, Kharkiv 61070, Ukraine*

Correspondence should be addressed to Parvathy Rajendran; aeparvathy@usm.my, Vijayanandh Raja; vijayanandh.raja@gmail.com, and Krishnakumar Kalaivani Muthuramalingam; k.kalaivani@student.khai.edu

Received 19 April 2023; Revised 15 July 2023; Accepted 8 September 2023; Published 26 September 2023

Academic Editor: Oronzio Manca

Natural fibre-reinforced polymer composites (NFRPs) have gained increasing attention in recent years as an alternative to conventional materials such as steel and aluminum alloys due to their ecofriendly, renewable, and low-cost nature. This paper focuses on the thermal application of NFRPs, which have shown great potential due to their good thermal insulation properties. In this study, the fabrication of jute and hemp fibre-reinforced composites, experimental testing, comparison, validation by using computational method, and proposed hemp NFRPs insulated exhaust pipe in place of conventional steel pipe. However, challenges such as moisture absorption and limited thermal properties on high thermal load still need to be addressed to enable the full-scale commercialization of NFRPs in thermal applications. For these comprehensive investigations, coupled and verified engineering approaches have been imposed. Fluid-thermal coupling has been executed in ANSYS workbench associated with conventional test outcomes. Through this approach, the low weight and low cost-based thermal load resisting material has been proposed for various engineering applications.

1. Introduction

Natural fibre has grown in popularity in recent years due to its low cost, abundance, nontoxic, and environmentally beneficial character. It is created by combining natural fibres such as jute, hemp, kenaf, cotton, silk, sisal, and others with a matrix material such as resin to form a material with stronger and additional mechanical and thermal qualities than the preceding raw materials. Natural fibre reinforcement polymers (NFRPs) have the ability to minimize energy consumption by reducing the work performed by the thermal system to recover the heat pulled out, as well as

greenhouse gas emissions and encourage sustainable development. In lower thermal loads, NFRPs provide a sustainable alternative to other insulation materials such as asbestos, polystyrene, and so on. The typical representation of prepared natural composite is revealed in Figure 1.

Natural fibre-reinforced composites are made by combining natural fibre in the reinforcing phase with a synthetic or bio-based polymer-based matrix in the matrix phase. Because it has a direct effect on the property of a composite product and renders it unsuitable for the desired use, the mixture would take place in the right proportion. Because of their advantages, such as being easily decomposable and ecofriendly, NFRPs will be used in thermal insulation in future industries such as aerospace, automobile, and chemical.

In the context of thermal systems such as exhaust, manifold insulation in vehicle sectors gives numerous benefits in terms of engine performance. The heat produced by the engine can be retained by insulating the exhaust pipe. This can help to raise the temperature of exhaust gases, where enhances gas flow out of the engine, particularly at lower RPMs. Exhaust gas temperature for varied petrol is taken from [1] and shown in Figure 2.

According to Arnau et al., insulation will aid in the combustion of unburned hydrocarbons emitted by the engine and thus minimize emissions [2]. Exhaust gas velocity is also boosted by retaining heat and lowering back pressure in the engine, which can result in improved performance and efficiency. However, it is dependent on the design of the bike engine.

Natural fibre composites have lesser thermal stability when compared to various types of synthetic fibres, and fibre deterioration owing to high thermal load will render NFRPs unsuitable for high temperature withstanding applications, particularly in higher cc bikes. Processing processes that include flame retardants have an effect on high thermal loads and thermal degradation.

1.1. Related Works. Muthukumar et al. investigated the usage of natural fibres such as banana, pineapple, and jute in various density combinations. 60% of the combinations used banana fibre, whereas the remaining 40% only used pineapple fibre. The increase in composite fibre thickness has an inverse relationship with the heat conductivity of the fibre combination. Maximum thermal resistance and lowest thermal conductivity were obtained when (C05) 60% banana, 32% pineapple, and 8% jute fibres were combined. Thermal conductivity and resistance of six combination fibre composites were investigated, and they demonstrated good insulation properties [3].

Venkatesan and Kadiresh produced a new jute reinforced composite material by combining three synthetic resins known for reduced thermal conductivity values of polymeric materials ranging from 0.1 to 0.5 W/mK with general-purpose resin, vinyl ester, isophthalic polyester, and cardanol. It has a few advantages over commonly used metals, including low density, high corrosion resistance, and inexpensive production costs. The effect of modifying each parameter was explored, and a regression equation was developed to identify whether composite material has good thermal properties. Thermal conductivity test results for the manufactured composite materials are range from 0.125 to 0.16 W/mK [4].

Figure 1: Jute fibre-reinforced composite.

Debnath researched jute fibre, which is less priced, yearly renewable, and commercially available than any other natural fibre crop. Jute farming is well known in Bangladesh and India. Hessian, carpet backing, and packaging (sacks) are a few well-known applications for fibre. Because of their lower cost and faster manufacturing method, synthetic fibres gradually surpassed traditional jute textiles in market share. It possesses thermal, electric, and acoustic resistant properties in various insulating forms [5].

Abedom investigated the fabrication of composite materials employing bamboo charcoal and bagasse fibre for technical uses by combining their diverse mechanical and thermal insulating capabilities. Five hybrid composites with various bagasse fibre/bamboo charcoal mixes are created using the compression molding procedure. ASTM techniques were used to evaluate the mechanical properties of the composite materials. The morphological test is used to analyze binding properties, internal fissures, and alignments. Tensile properties of natural fibre composites were found to be the same as those of artificial fibre composites. The insulating qualities of the natural fibre manufactured from bamboo with 30/70 charcoal were greater than those of other artificial fibres. The findings indicate the potential for employing these materials in component systems for automotive interiors [6].

Martin et al. used thermo gravimetric analysis, differential scanning calorimetry, and nitrogen and air atmospheres to investigate the thermal properties of raw and defatted sisal fibre. The atmosphere was a critical aspect in the DSC experiments that indicated the deteriorating process. In an inert environment, the DSC curve revealed distinct peaks for sisal fibres and their components. In the case of the air environment, all of the components' thermal curves displayed two exothermic peaks. In an inert environment, cellulose degrades via endothermic reactions, while in an atmosphere with air, it declines via exothermic processes. The elimination of lignin, as confirmed by TGA

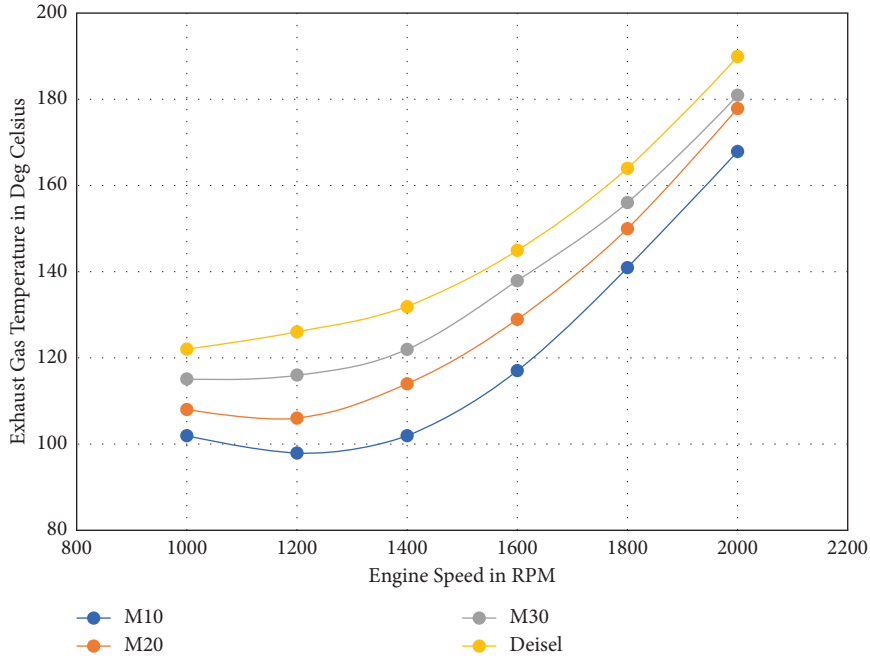

Figure 2: Exhaust gas temperature for varying fuel mixture.

tests, resulted in cellulose and hemicelluloses occurring at lower thermal loads than the raw form of sisal fibre [7].

Zhang et al. investigated the heat distribution and insulation behavior of a multilayered passive thermal protection system (MPTPS). The problem is that when exposed to high temperatures, the carbon-phenolic combination pyrolyzes, altering its thermal properties. The devolatilization of phenolic resin generates heat, which is absorbed by the carbon-phenolic compound. Tube furnace heating and Py-GC-MS experiments were used to investigate the pyrolysis properties of carbon-phenolic composites. The transient heat conduction process and many numerical computations supported the investigation of the effects on the insulating behavior of the passive system by negative heat source. The carbon-phenolic materials were pyrolyzed at 200°C, and the mass-loss rate increased to 25% when the heating temperature was raised to 900°C. Temperature rising point is delayed by increasing the wall thickness and negative heat source of the phenolic-carbon composited and has a large impact on outer wall temperature [8].

Awoyera et al. investigated the insulating and structural qualities of cement mortar supplemented with different mineral wool and fibre extracted from rice straw. The purpose was to see if adding mineral wool and rice straw would improve the thermal insulating qualities of Portland cement mortar. The mortar samples with dimensions of $40 \times 40 \times 160$ mm were reinforced with varied mineral wool and fibre from rice straw varying in bulk from 0% to 50% of weight. Water absorption, flexural and compressive strength, and thermal conductivity tests were performed on samples with and without the addition of mineral wool and rice straw. SEM was used to examine the microstructure of mortars. The heat conductivity of mortars decreased for reinforced mortars compared to cement with sand only. The inclusion of fibres delayed the mechanical characteristics of mortar, although the delay was not significant or fell short of acceptable standards [9].

Yusaf et al. evaluated the effect of methanol mixing ratios on engine performance. The mixing ratios were 10%, 20%, and 30% methanol. At various engine speeds, the performance of a four-stroke diesel engine was improved by altering the methanol mixture with fuel, and the reported exhaust temperature of a diesel-only engine was lower when compared to a blended fuel engine with improved performance. According to this study, adding 10% methanol to diesel fuel can have a considerable impact on both the environment and engine performance [1]. Saravanan et al. developed jute, pineapple, and banana fibre-based composites with different weight percentages. Composites with two fibres of equal weight percentage and different thicknesses of 5 mm, 10 mm, and 15 mm are utilized to insulate the generator exhaust pipe. This study was conducted normally, and the thermal characteristics of the insulated pipe were enhanced over the noninsulated pipe [10].

Kandylas and Stamatelos summarized the current state of knowledge about heat transport phenomena in vehicle exhaust systems. Experiment data from steady-state transient heat transfer measurements in automotive exhaust systems are provided and analyzed using a comprehensive transient computer model that covers the exhaust pipe by single wall and double wall with air filled configuration. This study hypothesized that insulating the exhaust gas pipes and manifolds would raise the temperature of the exhaust gas [11]. Krishnara et al. used FEM methods to analyze the exhaust manifold for several designs. The inclination of the manifold structure causes pressure drop and temperature loss, resulting in a low power output from the engine. Reduced tilt greatly increases temperature and pressure from

the preceding structure and power delivery from the engine [12]. Arnau et al. investigated exhaust thermal insulation using transient analysis. Exhaust ports and manifolds are insulated using various approaches. And it was concluded that insulation reduces fuel pollutants and CO emissions by 20% while increasing exhaust gas enthalpy [2].

1.2. Author Observation. The authors discovered that natural composites have poorer thermal conductivities than other metals such as steel and aluminim due to the presence of microstructures such as pores and voids. These microstructures cause thermal resistance and significantly impair heat transmission rate. Peak deterioration occurs in natural fibres at maximum temperatures ranging from 150°C to 360°C depending on fibre reinforcement. Natural composites with higher fibre content have lower thermal conductivity values because fibres have lower thermal conductivity. Thermal stability and maximum temperature capability can be improved by treating fibre with alkaline solution, filler materials, curing process, and reinforcing procedures. Table 1 displays the results of research papers [1, 3–9] that reported thermal conductivity values for several types of available fibre.

Authors concluded that NFRPs are mostly fit for lower thermal load applications. The detailed procedure involved in this work is revealed in Figure 3.

2. Methodologies

Heat transfer rate and conductivity properties must be examined to build the NFRP in a thermal field. A heat flow meter is used to investigate thermal conductivity and resistivity, as well as moisture absorption qualities. Validate the experimental results and the computational analysis performed on the experimental test specimen. Based on the low error percentage, a computational analysis on the exhaust pipe is performed, and a grid convergence study is performed to improve the accuracy of the results [2, 13–26].

2.1. Experimental Studies

2.1.1. Material Selection. According to Table 1, it can be observed that Kenaf, Sisal, and cotton fibres have much lower thermal conductivity values in comparison to the other types of fibres. However, the availability, fabric preparation, and extraction cost of these fibres are significantly elevated.

2.1.2. Test Material Preparation. The raw jute and hemp fibres have a diameter of 10 microns and 25 microns, respectively, and are treated and woven into a sort of bidirectional fabric. Jute has a layer thickness of 0.84 mm, while hemp has a thickness of 0.89 mm. If there were 8 layers of hemp fabric, the total thickness would be 7.12 mm, and if there were 9 layers of jute fabric, the total thickness would be 7.56 mm. The results of a mixture of epoxy resin and aromatic amine hardener with the proportion of 10 : 2 as weighted shown in Figure 6 are presented.

The ratio of fibre to resin in the mixture is exactly 50/50. The conventional method of hand-layup is utilized throughout the production of test materials. The mold is prepared for the first time for the insertion of the fibres. The resins are then subjected to an impregnation process, during which rollers, brushes, or several other types of impregnators are utilized. After going through this procedure, the laminates that were created are subsequently cured using

Table 1: Thermal conductivity values for varying density and matrix phase.

Natural fibre	Thermal conductivity (W/mK)
Banana	0.12–0.6
Bamboo	0.1–1.8
Hemp	0.2–1.6
Jute	0.1–1.5
Cotton	0.12–0.5
Kenaf	0.09–0.75
Sisal	0.1–0.9

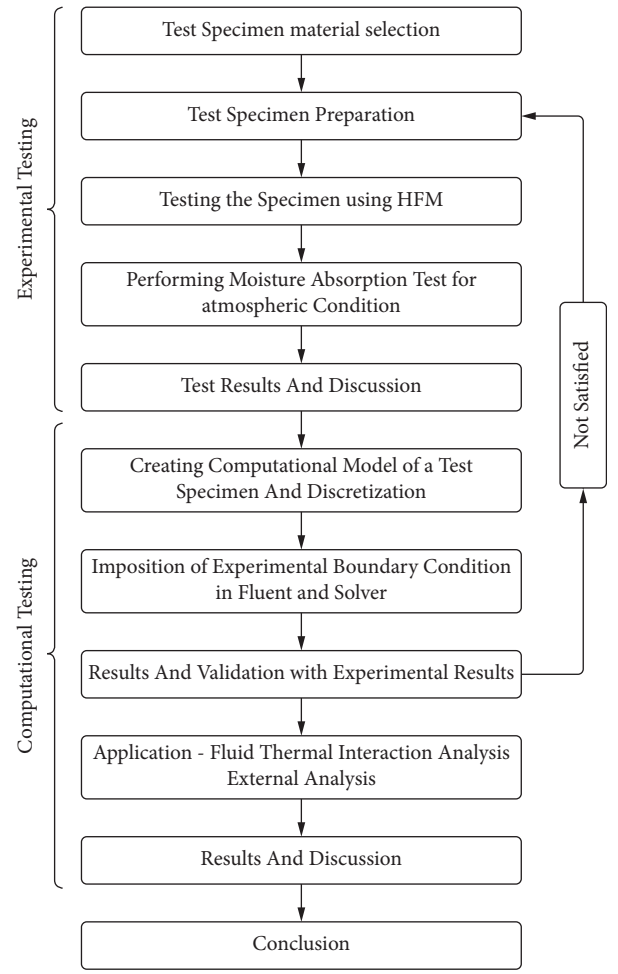

Figure 3: Postulates employed by the authors to conclude the NFRPs in thermal application.

Figure 4: Jute fabric for experimental test specimen preparation.

Figure 5: Hemp fabric for experimental test specimen preparation.

Figure 6: Measurements of epoxy-resin for experimental test specimen.

standard atmospheric conditions. In a manner analogous, six layers of hemp are utilized in order to achieve a composite thickness of 12 mm. The fully constructed model of a square plate made of hemp may be shown in Figure 7 [2, 13–26].

2.1.3. Test Apparatus-HFM. In accordance with ISO 8301 : 1991, a heat flow meter can be used to determine the thermal properties of the test material, such as the thermal conductivity and thermal resistivity of the material. According to the instructions provided by the heat flow

Figure 7: Hemp-fabricated test specimen.

meter, the testing material is sliced into pieces of 300 by 300 mm with a user-specified thickness of 12 mm before being placed in a heat flow meter apparatus consisting of a heated plate and temperature sensors that were in contact with the testing material. The thermal conductivity and resistance of the test material are both determined by making use of the difference in temperature that is measured between the two sensors [2, 13–26].

2.1.4. Moisture Absorption Test. The method that is given in ASTM D 579-99 procedures is used to determine the moisture absorption capabilities of hemp and jute fibre reinforced composites. The relationship of water absorption is expressed in the following equation:

$$\text{WaterAbsorption}\,(\%) = \frac{(\text{Wetweight} - \text{Reconditionedweight})}{\text{Reconditionedweight}} \times 100. \quad (1)$$

From the composite, test specimens with the dimensions of $25.4 \times 76.2\ \text{mm}^2$ and a thickness of 12 mm are cut, and the results of the measurements taken are presented in Figure 8. The samples are then promptly dried before being weighed. In order to get an accurate reading of the water absorption, test materials are submerged in water for varied amounts of time while their restored weights are recorded [2, 13–26].

2.1.5. Test Results. HFM is used to conduct tests on a fabricated jute and hemp fibre reinforced composite with dimensions of 300 mm × 300 mm and a thickness of 12 mm in order to examine heat convection. The test is carried out with a temperature difference of 10 degrees Celsius and a constant temperature of 80 degrees Celsius. Based on the findings, the thermal conductivity and resistivity of jute NFRP have been determined to be $0.14873\,W/\text{mK}$ and $0.08119\,m^2/\text{mK}$. Similarly, for hemp NFRP, the thermal conductivity and resistivity values are found as $0.122702\ W/\text{mK}$ and $0.098422\ m^2/\text{mK}$. The comprehensive experimental test based outcomes of thermal conductivity and resistivity are revealed in Figure 9 [2, 13–26].

Utilizing equation (1), a determination can be made on the percentage of moisture absorbed by the test specimen. Figure 10 presents a plot of the findings of the experiment.

The NFRP of hemp can absorb up to 0.99% of its body weight, while the NFRP of jute can absorb up to 5.39% of its body weight.

2.2. Computational Thermal Analysis

2.2.1. Computational Plate Model. The composite plate constructed of jute and hemp fibre is the physical representation of this problem in the computational model. Figure 11 depicts a composite plate that measures 300 mm on each side and has a thickness of 12 mm. For the purpose of designing the computational model, the Ansys Design-Modeler workbench is utilized [27–30].

After the model has been created, the material properties of the hemp and jute are derived from the experimental data reported in Table 2 and then supplied into the model as material input data.

2.2.2. Discretization. The continuous domain is discretized using either finite elements or discrete elements when computational models are used. Structured meshing takes the place of adaptive meshing when it is applied to a surface that has been subdivided into a grid of square elements. The generation of a mesh that has sufficient density to faithfully depict the plate's overall heat flux is the objective of the discretization process. The underlying mesh structure of the plate is shown in Figure 12 [27–30].

2.2.3. Boundary Condition. The Dirichlet boundary condition is applied, and both the starting and ending temperatures are held at a constant value across the boundaries. One side of the material has a thermal load of 80 degrees Celsius applied to it, while the other side has a thermal load of 70 degrees Celsius applied. In addition, the state of the remaining faces is maintained to be adiabatic. Figure 13 illustrates the model with the boundary condition added in [27–30].

2.2.4. Solver Data and Equations. The convection–diffusion equation is an equation that conserves both energy and mass and is responsible for governing the convective heat transfer. The equation for the general form of energy conservation in convective heat transfer is as follows:

Figure 8: Measurements of hemp NFRPs made with ASTM standard.

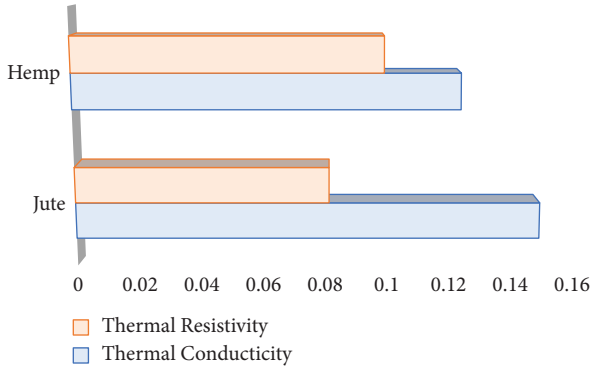

Figure 9: Variation of thermal conductivity and resistivity between jute and hemp NFRPs.

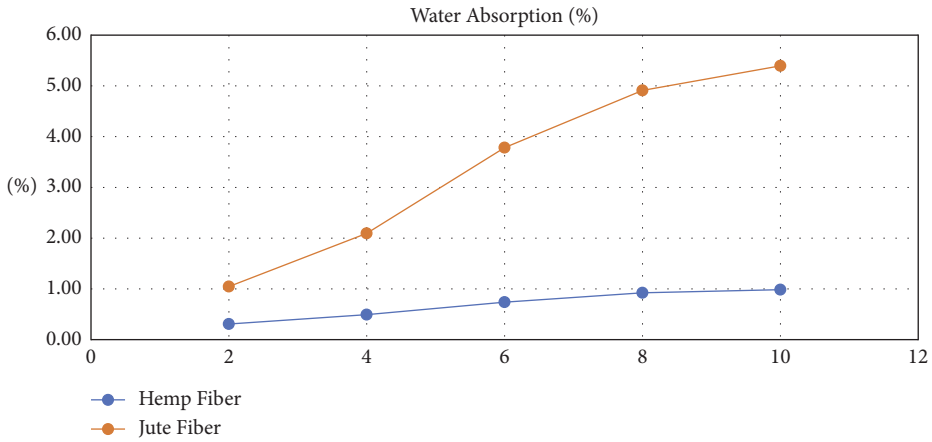

Figure 10: Moisture abortion in % between jute and hemp NFRPs.

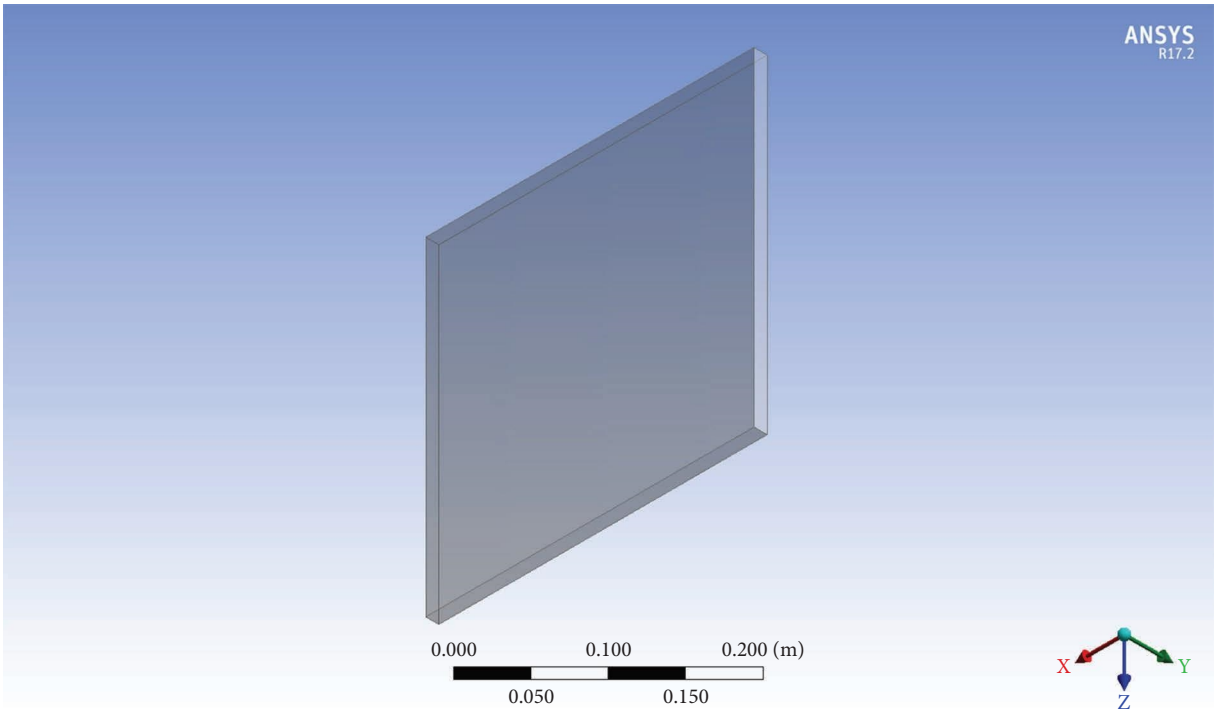

Figure 11: Computational plate model for testing.

Table 2: Properties of the materials.

Material	Isotropic thermal conductivity (W/mK)
Jute	0.14873
Hemp	0.122702

$$\frac{\partial(\rho c_T)}{\partial T} + \nabla * (\rho c_T * U) = \nabla * (K.\nabla T) + Q, \tag{2}$$

where $\partial(\rho c_T)/\partial T$ is the time rate change of energy within the domain, T is the temperature of the medium, ∇ is denoted as divergence factor, v is the velocity vector of the fluid, $\nabla * (\rho c_T u)$ is represented as convective term that accounts the amount of heat transported by convection, $\nabla * (k.\nabla T)$ is represented as diffusive term that accounts the amount of heat transported by diffusion, ΔT is the temperature difference between the boundaries, and Q is denoted as the source/sink term [27–30].

2.2.5. Result and Validation. The findings of the thermal analysis performed on the composite plates for the experimental boundary condition are withheld. Figure 14 illustrates the temperatures that were applied at both of the limits. It would appear that the heat flux for the jute NFRPs is 123.94 $\mathbf{W/m^2}$ and for hemp NFRPs is 102.25 94 $\mathbf{W/m^2}$. Figures 15 and 16 present the computational findings obtained for the two plates, respectively. The amount of heat transported by jute NFRPs is 11.155 watts, while the amount transferred by hemp NFRPs is 9.20 watts [27–30].

Experimental test results show the thermal conductivity of jute and hemp NFRPs are 0.14873 W/mK and 0.122702 W/mK for mean temperature 80 Degrees Celsius and temperature difference of 10°C. With this data, heat transfer and heat transfer rate can be calculated by using the following formula:

$$Q = \frac{k * \Delta T * A}{D}, \tag{3}$$

where Q is the heat transferred amount, k is denoted as thermal conductivity in W/mK, ΔT is the temperature difference between the two surfaces, A is the cross-sectional area, and D is represented as thickness of the specimen [27–30].

Heat transferred for jute NFRPs can be calculated as follow, the values of jute NFRPs are $k = 0.14\,W$/mK, $\Delta T = 283$ k, $D = 0.12$ m, and $A = 0.036$, where

$$Q = \frac{0.14 * 283 * 0.036}{0.12} = 11.886\,W. \tag{4}$$

For hemp NFRPs $k = 0.12$, where

$$Q = \frac{0.12 * 283 * 0.036}{0.12} = 10.18\,W. \tag{5}$$

It would appear that the error percentage while validating experimental and computational data is less than 10%. This suggests that the experimental test specimen may have discontinuity, inappropriate resin fibre contact, and poor resin fibre fusion, all of which vary according to the preparation and curing method. The insulation of the real-world problem can be solved by using the solutions that were collected and validated [27–30].

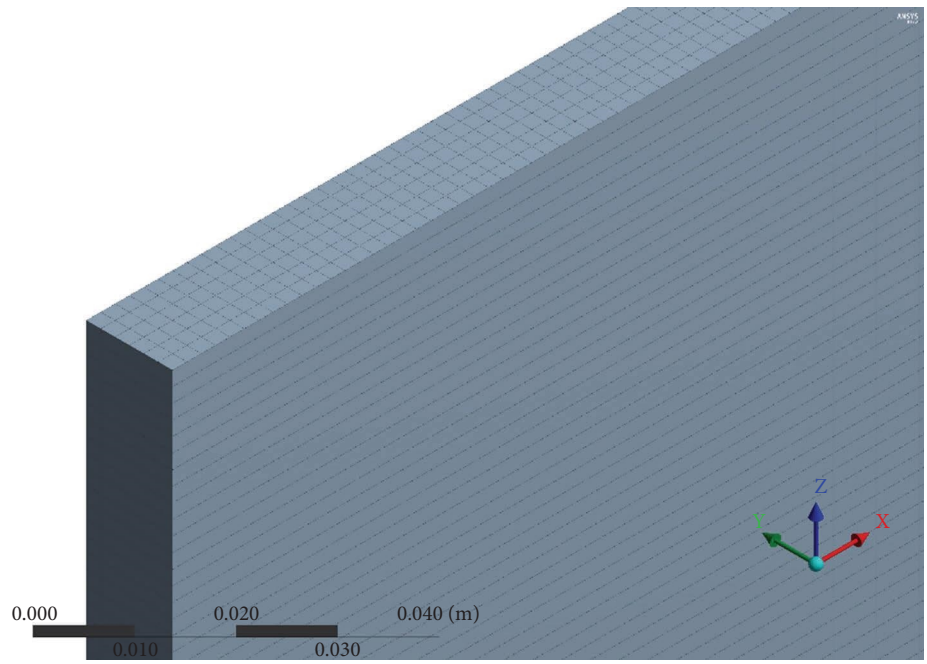

Figure 12: Structured mesh of computational plate mode.

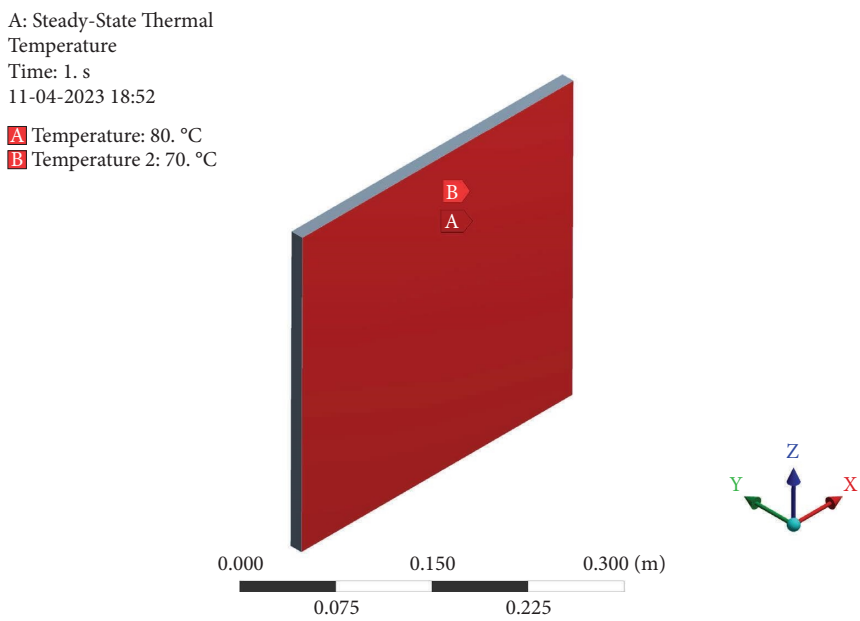

Figure 13: Computational model imported with experimental test data as boundary condition.

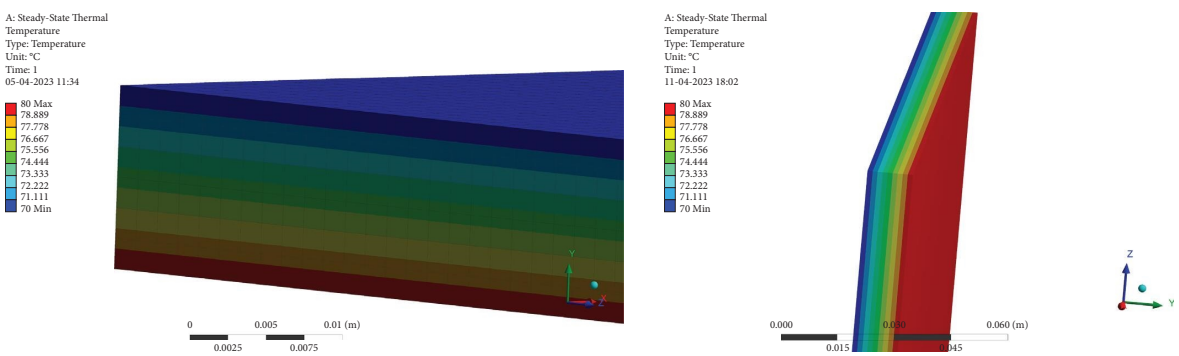

Figure 14: Applied thermal load 80°C with a temperature gradient of 10°C.

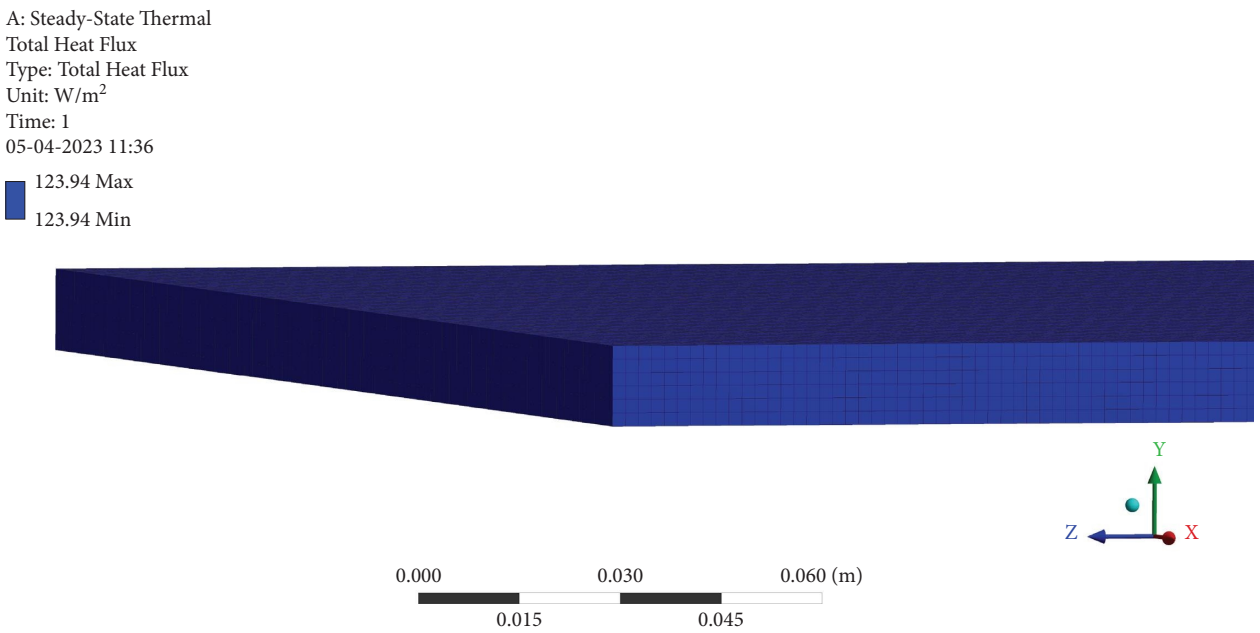

Figure 15: Uniform distribution of heat flux over the jute NFRPs properties imported computational model.

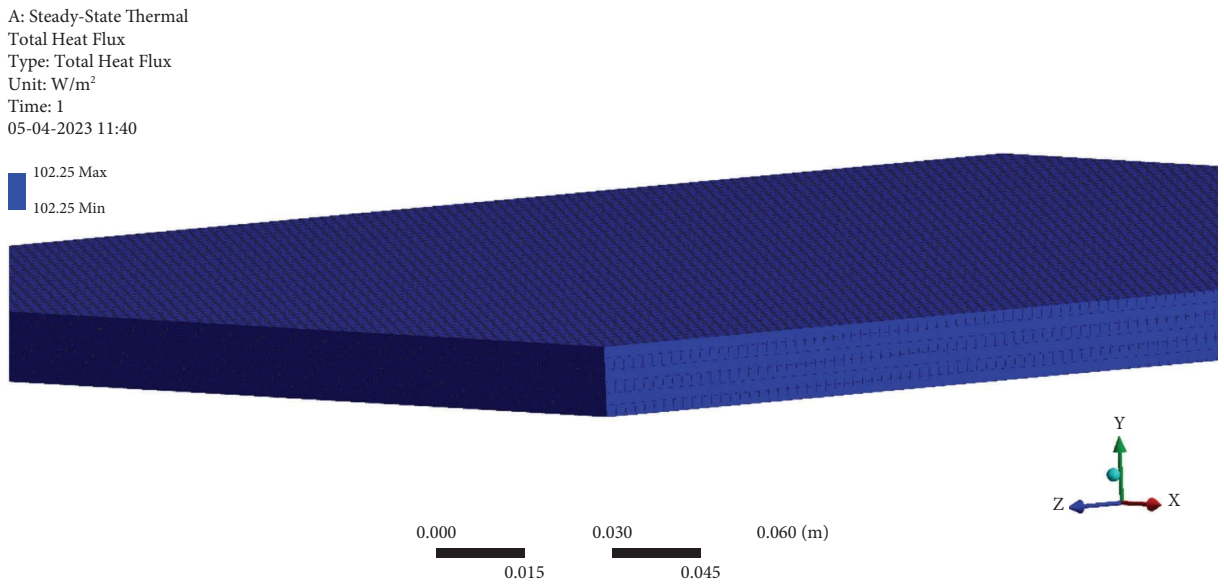

Figure 16: Uniform distribution of heat flux over the hemp NFRPs properties imported computational model.

2.3. Fluid-Thermal Interaction Analysis for Real-Time Engineering Problems

2.3.1. Computational Domain and Discretization. The universal exhaust pipes of a 4 stroke engine are the subject of this instance's computationally defined model. Fusion 360 is used to develop the 3D model of the universal fitting exhaust pipe, and then that model is transferred into the Ansys fluent programme. Figure 17 reveals computational simulations of the exhaust pipe for a four-stroke engine. Ansys design modeler is utilized in order to produce a fluid domain. The closeness and curvature size functions are then used to discretize the computational fluid domain into fine triangular and tetrahedral parts. Figure 18 demonstrates how the meshed structure of the computational model may be seen [27–30].

2.3.2. Boundary Conditions. For discretized model, inlet velocity is found by using volumetric flow rate from the engine cylinder as follow.

Given the specifications of a Honda CB 200's 200cc motorcycle engine, namely, a stroke length of 63mm and a bore diameter of 61mm, operating at a rotational speed of 6000 RPM, we can analyse the performance characteristics of this four-stroke engine. This implies that there are 3000 exhaust strokes occurring within a minute.

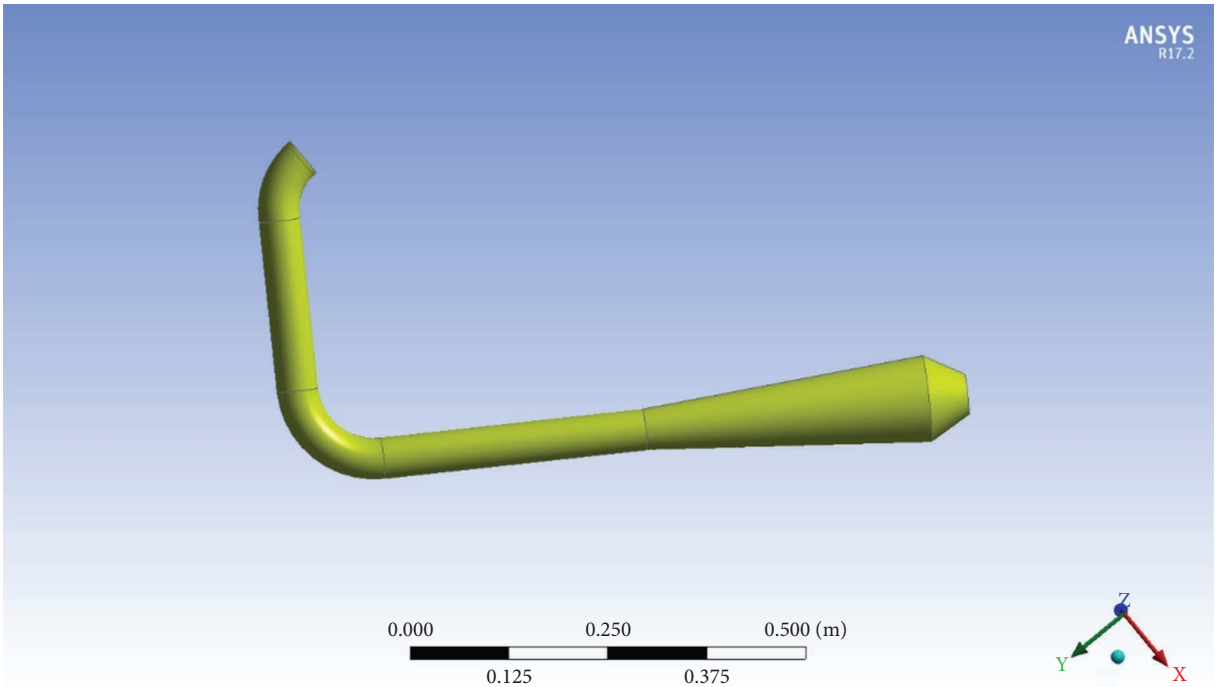

Figure 17: 4 Stroke engine exhaust pipe.

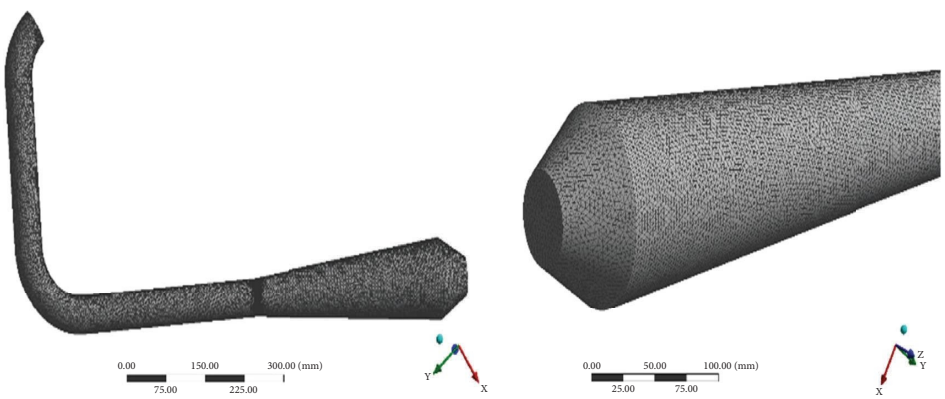

Figure 18: Meshed structure of the exhaust model.

$$\text{Volume (in cc)} * \text{Exhaust strokes} = 200\text{cc} * 3000 = \frac{6{,}00{,}000\ \text{cc}}{\text{min}}. \tag{6}$$

Volumetric flow rate of exhaust gas is calculated as 0.0100 m^3/sec.

At 6000 RPM, piston completes 12000 strokes per minute, velocity can be found by using the following equation:

$$\left(\frac{63}{1000}\right)m * \left(\frac{12000}{60}\right)\frac{\text{stokes}}{s} = 12.6\ \frac{m}{s}. \tag{7}$$

The bore diameter of cylinder is 61 mm. Area at cylinder exit is as follows:

$$\frac{\pi}{4} * \left(61^2\right) = 2924.7\ \text{mm}^2. \tag{8}$$

Diameter at exhaust exit tip is 31.5 mm and the area is calculated by using the following equation:

$$\frac{\pi}{4} * \left(31.5^2\right) = 779\ \text{mm}^2. \tag{9}$$

By using continuity equation, exit velocity can be calculated as follows:

$$A_1 v_1 = A_2 v_2$$
$$v_2 = \frac{(2924.7) * 12.6}{779} = 47.3\ \frac{m}{s}. \tag{10}$$

The inlet of the discretized model is the velocity inlet, and the average exhaust gas temperature from [1] of 393 k is fed as boundary condition for the inlet. The outlet of the model is a pressure outlet, and the magnitude of pressure is 101325 Pa. Conditions for the wall are no slip, stationary wall equipped with convective heat transfer of default thermal conductivity value of steel as 16.27 W/mK, and ambient temperature of 288.16 K [27–30].

2.3.3. Solver Data and Equations. For fluid analysis through the domain of the exhaust, working fluid is chosen as air treated as ideal gas.

$$\rho = \frac{p_p + p}{R/M \times T_0}, \tag{11}$$

where ρ is denoted as the density of working fluid, p_p is denoted as operating pressure, p is denoted as static pressure, R is represented as universal gas constant, M is represented as molecular weight of air, and T_0 is denoted as local temperature [27–30].

Viscosity depends on temperature to consider this, Sutherland's law and its models is employed as follows:

$$\mu_0 = \mu_1 \left(\frac{\mathrm{T}}{\mathrm{T}_0}\right)^{3/2} \frac{\mathrm{T}_1 + \mathrm{S}}{\mathrm{T}_0 + \mathrm{S}}, \tag{12}$$

where μ_0, μ_1, T_1, and S are denoted as viscosity of working liquid, reference viscosity, reference temperature at sea level, and Sutherland constant, respectively.

The three coefficient of Sutherland's law default values for air is as follows:

$$T_1 - 273.11\,K, \mu_1 - 1.716 \times 10^{-5} \frac{\mathrm{kg}}{\mathrm{ms}}, \mathrm{S} - 110.56\,K. \tag{13}$$

The governing equation of continuity, momentum, and energy relation for this case is as follows:

$$\begin{aligned} \nabla.(\rho.\vec{v}) &= 0, \\ \nabla.(\rho * \vec{v} * \vec{v}) &= -\nabla p + \nabla.(\tau) + S_V, \\ \nabla.(\vec{v}(\rho.E + p)) &= \nabla.\left(k_{\mathrm{eff}}.\nabla T\right) + S_H, \end{aligned} \tag{14}$$

where $\vec{v}$, τ, E, k_{eff}, and S_H are represented as velocity vector, stress tensor, internal energy, effective conductivity of the fluids, and energy source term [27–30].

Turbulence effects are included by deploying $k - \varepsilon$ model. Governing equation for $k - \varepsilon$ model is provided as follows:

$$\begin{aligned} \frac{\partial}{\partial x_i}(\rho \mathrm{k} u_i) &= \frac{\partial}{\partial x_i}\left[\left(\mu_0 + \frac{\mu_t}{\sigma_k}\right)\frac{\partial k}{\partial x_j}\right] \\ &\quad + G_k + G_b - \rho\varepsilon - Y_M + S_k, \\ \frac{\partial}{\partial x_i}(\rho \varepsilon u_i) &= \frac{\partial}{\partial x_i}\left[\left(\mu_0 + \frac{\mu_t}{\sigma_\varepsilon}\right)\frac{\partial \varepsilon}{\partial x_j}\right] \\ &\quad + C_{1\varepsilon}\frac{\varepsilon}{k}\left(G_k + C_{3\varepsilon}G_b\right) - C_{2\varepsilon}\rho\frac{\varepsilon^2}{k} + S_\varepsilon, \end{aligned} \tag{15}$$

where k is denoted as turbulence kinetic energy, k is denoted as turbulence dissipation rate, G_k and G_b are the turbulence kinetic energy created due to velocity gradients and buoyancy, Y_M is represented as dilation fluctuation in compressible turbulence to overall dissipation rate, μ_t, σ_k, and σ_ε are the eddy viscosity and turbulent Prandtl number for k and ε, S_k and S_ε are the source terms, and $C_{1\varepsilon}, C_{2\varepsilon}$, and $C_{3\varepsilon}$ are the constants [27–30].

2.3.4. Grid Convergence Study. The study of grid convergence offers a clearer comprehension of how the results of computations are influenced by the size of their constituent elements. There are eight distinct situations, each consisting of a different element size, capturing proximity with or without the element, curvature size functions, minimizing element size, and doing analysis. The maximum temperature and the minimum temperature are the two factors that are taken for the computational model which is taken for the study. Taking these two parameters helps enhance accuracy and provides a dependable output. The results are presented in the form of a graph, which can be found in Figures 19 and 20, respectively.

Figures 19 and 20 show the highest and minimum temperatures at which saturation occurs for a range of element sizes. Saturation is reached at 850958 elements and the results are analyzed for the steel, hemp, and jute properties-imposed model. At 850958 elements, saturation is achieved. The maximum temperature at saturation is 393.329 K, and the minimum is 363.299 K.

Case 1: Number of elements: 443593; maximum and minimum attained temperatures are 393.228 K and 368.497 K, respectively. Results for Case 1 are revealed in Figure 21.

Case 2: Number of elements: 562650; maximum and minimum attained temperatures are 393.298 K and 367.050 K, respectively. Results for Case 2 are revealed in Figure 22.

Case 3: Number of elements: 2013664; maximum and minimum attained temperatures are 393.359 K and 361.843 K, respectively. Results for Case 3 are revealed in Figure 23.

3. Results and Discussion

3.1. Results from Computational Study. Because of this work, NFRPs can now be used as an insulating material in bike exhaust systems. The heat transfer to the surrounding environment is investigated using jute and hemp NFRPs as well as traditional steel exhaust pipes for comparison. Figures 24 and 25 present the findings that were obtained when the specified boundary condition was applied.

The results from the fluent are input into the steady state thermal model in order to calculate the quantity of heat transmitted and the heat flux. Figure 26 presents the imported results of temperature measurements taken from the fluid domain. This can be carried out in accordance with the manner described in Section 2.2.

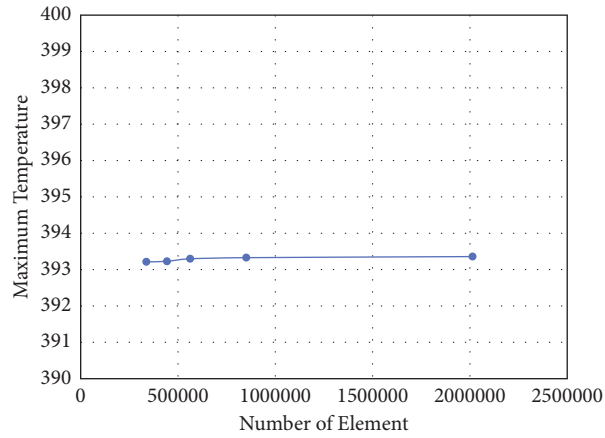

Figure 19: Grid convergence study for varying element size and maximum temperature is plotted.

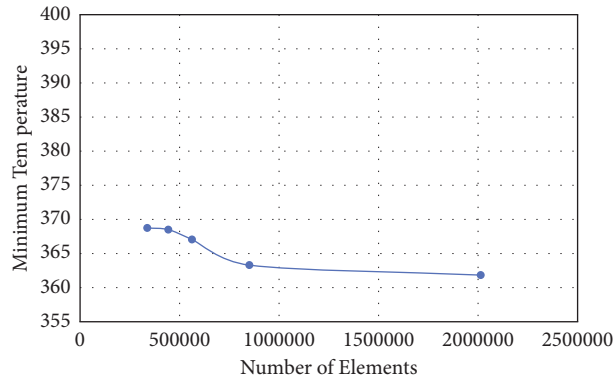

Figure 20: Grid convergence study for varying element size and minimum temperature is plotted.

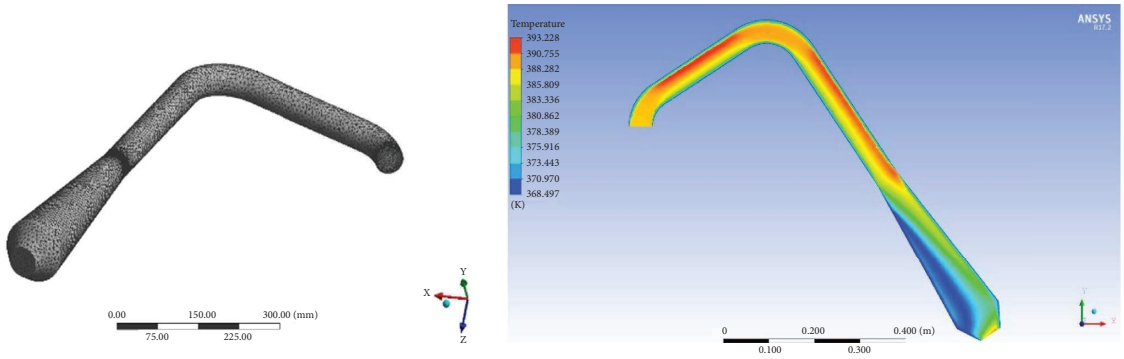

Figure 21: Meshed structure and temperature results for 443593 mesh elements.

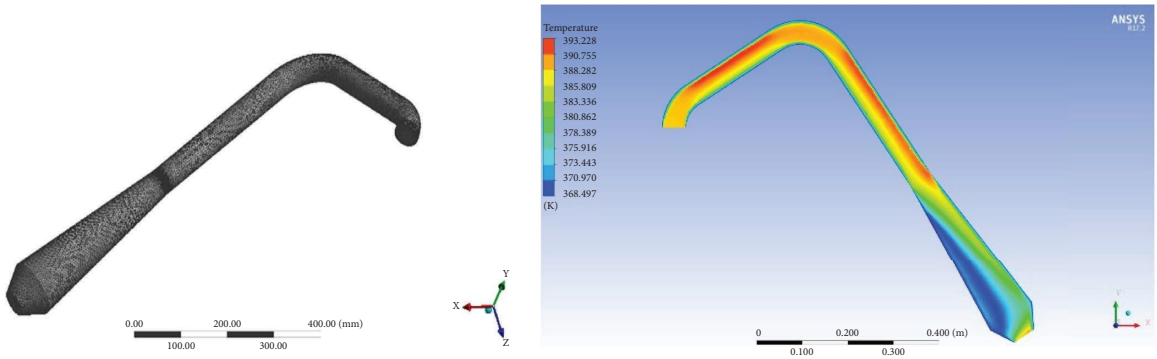

Figure 22: Meshed structure and temperature results for 562650 mesh elements.

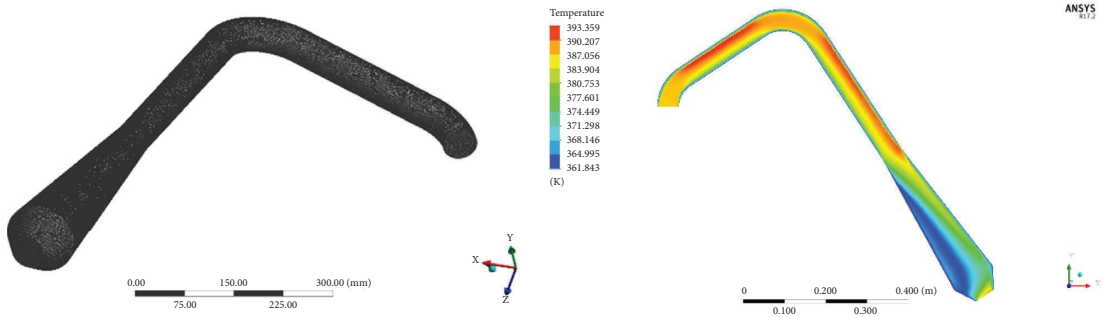

Figure 23: Meshed structure and temperature results for 2013664 mesh elements.

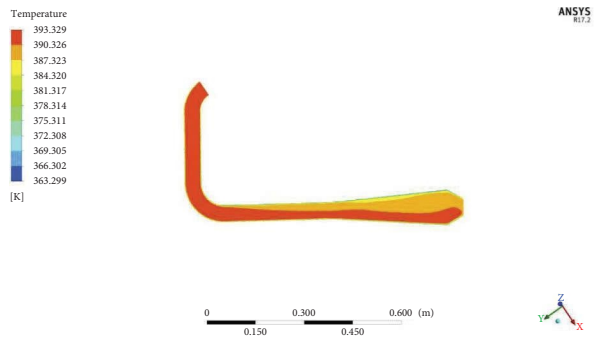

Figure 24: Temperature of fluid created for exhaust pipe.

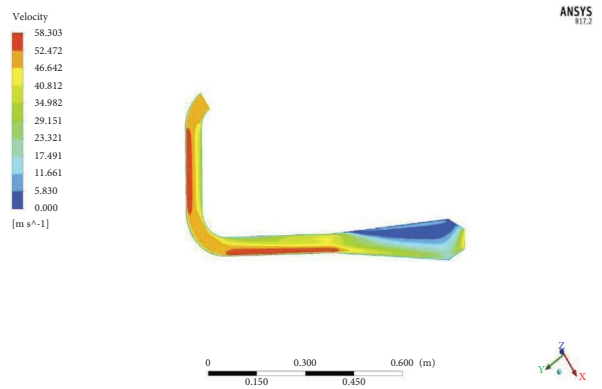

Figure 25: Velocity of fluid domain created for exhaust pipe.

In addition, steel is incorporated so that the results may be compared with those of NFRP materials made of jute and hemp. Figure 27 illustrates the heat flow that was imported from a model containing steel's characteristics. Figure 28 presents the heat flux that is disclosed by the hemp NFRPs properties-imposed model. Figure 29 illustrates the heat flux that is caused by the properties-imposed model for jute NFRPs.

In comparison to steel and jute NFRPs, the quantity of heat that is transferred by convection through hemp NFRPs is much lower. Figure 30 depicts a plot of the difference in

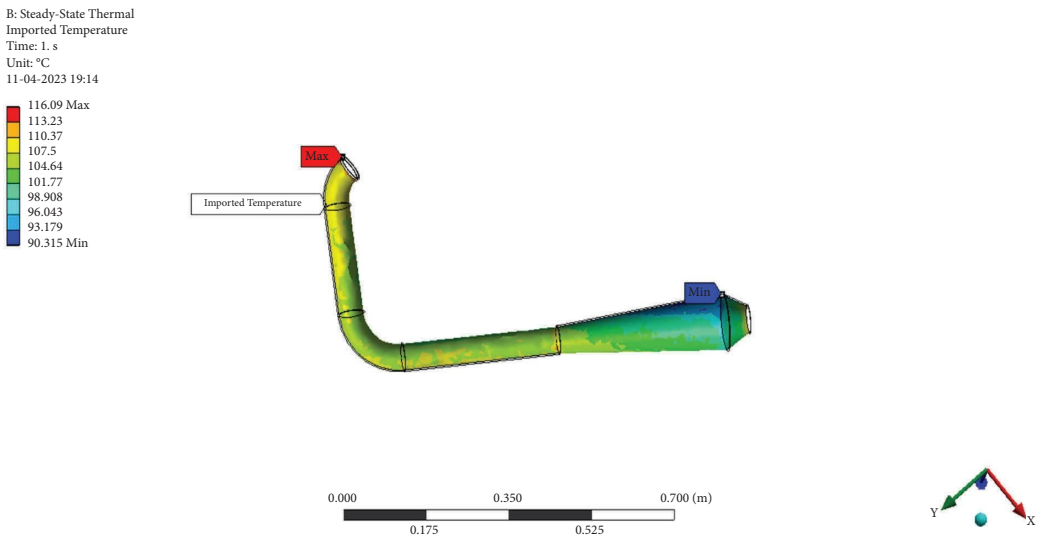

Figure 26: Imported load from the fluid domain.

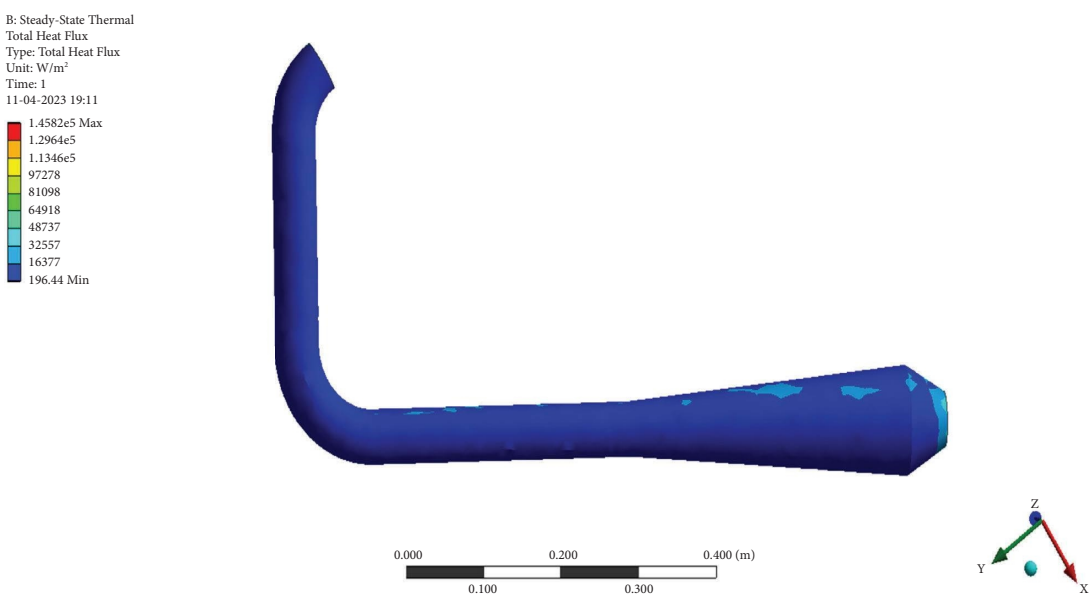

Figure 27: Heat flux for steel properties-imposed model.

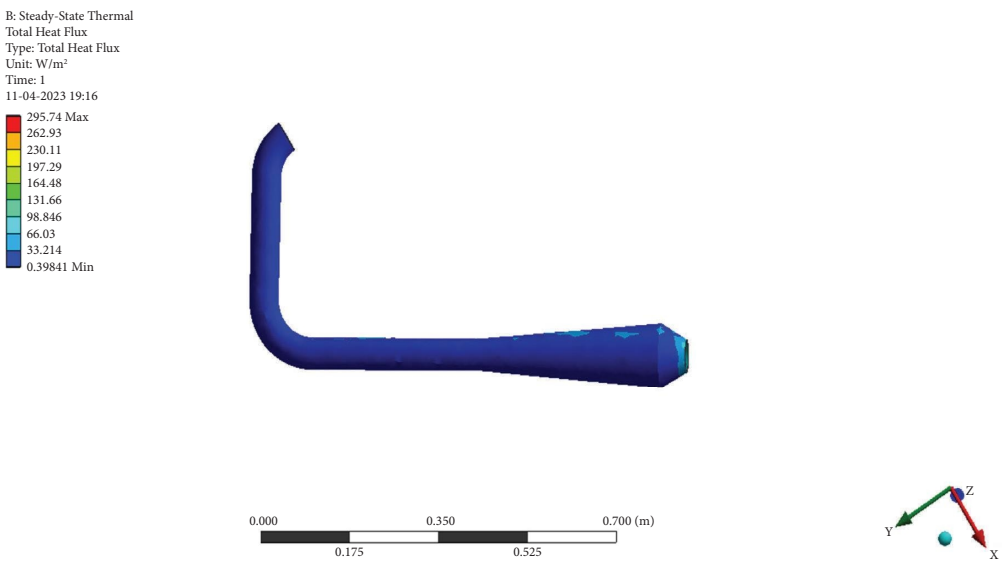

Figure 28: Heat flux for hemp NRPF properties-imposed model.

Figure 29: Heat flux for jute NRPF properties-imposed model.

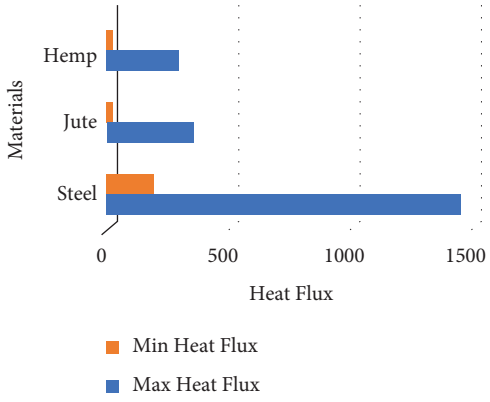

Figure 30: Comparison of heat flux between steel, hemp NRPFs, and jute NRPFs.

heat flux that occurs between NFRPs made of steel, jute, and hemp.

4. Conclusion

Hemp and jute are selected with the assistance of a literature review on the basis of their availability, the cost of processing, and their thermal performance. It is possible to successfully manufacture composite material that is reinforced with jute and hemp fibres. The constructed model is put through a thermal test in steady state, and observed thermal load transfer is carried out. When subjected to a moisture absorption test in order to determine the capability of capturing moisture, the results showed that hemp NFRPs had a lower level of moisture absorption in comparison to jute NFRPs. Additionally, the heat transmission in hemp NFRPs was quite low. The use of computational tools allows for this assertion to be properly confirmed.

The exhaust model is evaluated computationally to ensure that there is minimal error based on the results of the computations. The velocity and temperature of exhaust gas are estimated using an analytical approach and reviews of the relevant literature. For the sake of computational investigation, these values are employed. A grid convergence research is carried out in order to guarantee the precision of the CFD. The findings from the jute and hemp NFRPs were compared with those from typical steel pipes, and it was discovered that the hemp NFRPs are best suited for lower thermal loads and have lower heat transfer values.

The primary focus of future study will be on the development of composites, namely, by altering the fibre-to-resin ratio and combining fibre pavement with alkaline materials in an effort to improve the thermal resistance of NFRP composites. In terms of the insulation, the analysis would need to be carried out in a transient state in order to monitor the thermal performance of the composite brought about by varying flow parameters using computational methods.

The commercialization of hemp natural fibre reinforced plastics (hemp NFRPs) in low thermal environments involves the study of additional characteristics such as thermal deterioration and the treatment of fibres prior to manufacture in order to increase thermal behavior.

Data Availability

The data supporting the findings of this study are available within the article.

Conflicts of Interest

The authors declare that they have no conflicts of interest.

Acknowledgments

The authors acknowledge that this study has been performed based on the authors' interests, and it makes use of the computational resources and experimental resources from the design and simulation laboratory and the aerodynamics laboratory at Kumaraguru College of Technology, Coimbatore, Tamil Nadu, India.

References

[1] T. F. H. Yusaf, I. Baker, and P. Najafi, "Gholamhassan 1395 the effect of methanol-diesel blended ratio on CI engine performance," *International Journal of Automotive and Mechanical Engineering*, vol. 8, 2013.

[2] F. J. Arnau, J. Martín, P. Piqueras, and Á. Auñón, "Effect of the exhaust thermal insulation on the engine efficiency and the exhaust temperature under transient conditions," *International Journal of Engine Research*, vol. 22, no. 9, pp. 2869–2883, 2020.

[3] K. Muthukumar, R. V. Sabariraj, S. Dinesh Kumar, and T. Sathish, "Investigation of thermal conductivity and thermal resistance analysis on different combination of natural fiber composites of Banana, Pineapple and Jute," *Materials Today: Proceedings*, vol. 21, pp. 976–980, 2020.

[4] S. P. Venkatesan and P. N. Kadiresh, "Investigations on thermal properties of biodegradable and environment friendly composite materials for insulation in thermal systems," *Energy Sources, Part A: Recovery, Utilization, and Environmental Effects*, vol. 43, 2019.

[5] S. Debnath, "Thermal insulation material based on "jute"" *Insulation Materials In Context Of Sustainability*, IntechOpen, London, UK, 2016.

[6] F. Abedom, S. Sakthivel, D. Asfaw, B. Melese, E. Solomon, and S. S. Kumar, "Development of natural fiber hybrid composites using sugarcane bagasse and bamboo charcoal for automotive thermal insulation materials," *Advances in Materials Science and Engineering*, vol. 2021, Article ID 2508840, 10 pages, 2021.

[7] A. R. Martin, M. A. Martins, O. R. R. F. Da Silva, and L. H. C. Mattoso, "Studies on the thermal properties of sisal fiber and its constituents," *Thermochimica Acta*, vol. 506, no. 1-2, pp. 14–19, 2010.

[8] X. Zhang, Y. Wang, Y. Wang, B. Liu, and X. Bai, "Preliminary study on the thermal insulation of a multilayer passive thermal protection system with carbon-phenolic composites in a combustion chamber," *Case Studies in Thermal Engineering*, vol. 35, Article ID 102120, 2022.

[9] P. O. Awoyera, A. D. Akinrinade, A. G. De Sousa Galdino, and F. Althoey, "Thermal insulation and mechanical characteristics of cement mortar reinforced with mineral wool and rice straw fibers," *Journal of Building Engineering*, vol. 53, Article ID 104568, 2022.

[10] A. K. Saravanan, A. Rajendra Prasad, D. Muruganandam, G. Saravanan, S. Vivekanandan, and M. Sudhakar, "Study on natural fiber composites of jute, pine apple and banana compositions percentage of weight basis for thermal resistance and thermal conductivity," *Materials Today: Proceedings*, vol. 37, pp. 147–151, 2021.

[11] I. P. Kandylas and A. Stamatelos, "Engine Exhaustsystem design based on heat transfer computation," *Energy Conversion and Management*, vol. 40, no. 10, pp. 1057–1072, 1999.

[12] C. Krishara J, S. Rajesh Ruban, and N. Subramani, "Analysis of exhaust manifold to improve the engine performance," *International Journey Of Engineering*, vol. 7, no. 2, p. 8, 2018.

[13] A. Chatterjee, S. Kumar, and H. Singh, "Tensile strength and thermal behavior of jute fibre reinforced polypropylene laminate composite," *Composites Communications*, vol. 22, no. 2020, Article ID 100483, 2020.

[14] E. Sinha and S. K. Rout, "Influence of fibre-surface treatment on structural, thermal, and mechanical properties of jute fibre and its composite," *Bulletin of Materials Science*, vol. 32, no. 1, pp. 65–76, 2009.

[15] F. Chegdani, M. El Mansori, S. T. S. Bukkapatnam, and I. El Amri, "Thermal effecton the tribo-mechanical behavior of natural fiber composites at micro-scale," *Tribology International*, vol. 150, pp. 1–7, 2019.

[16] M. K. Huda and I. Widiastuti, "Natural fiber reinforced polymer in automotive application: a systematic literature review," *Journal of Physics: Conference Series*, vol. 1808, no. 1, Article ID 012015, 2021.

[17] J. Zach, V. Novak, and J. Peterkova, "Study of the behaviour of thermal insulation materials made with recycled textile fibers," *IOP Conference Series: Materials Science and Engineering*, vol. 385, Article ID 012065, 2018.

[18] T. F. H. Yusaf, I. Baker, and P. Najafi, "Gholamhassan 1395 the effect of methanol-diesel blended ratio on CI engine performance," *International Journal of Automotive and Mechanical Engineering*, vol. 8, 2013.

[19] D. Anand and V. Suresh, "Design and analysis of exhaust manifold," *International Research Journal of Multidisciplinary Technovation*, vol. 2, pp. 1–8, 2020.

[20] S. S. Yoon, K.-O. Lee, S.-B. Lee, and K. Park, "Thermal stress and fatigue analysis of exhaust manifold," *Key Engineering Materials*, vol. 261, pp. 1203–1208, 2004.

[21] S. Martínez-Martínez, R. Leal-Garza, F. Sánchez-Cruz, and V. Esteban, "CFD analysis of the effect of the exhaust manifold design on the close-coupled catalytic converter performance," *Journal of KONES*, vol. 17, pp. 303–311, 2010.

[22] J. S. S. Neto, H. F. M. de Queiroz, R. A. A. Aguiar, and M. D. Banea, "A review on the thermal characterisation of natural and hybrid fiber composites," *Polymers*, vol. 13, p. 4425, 2021.

[23] T. P. Sathishkumar, P. Navaneethakrishnan, S. Shankar, R. Rajasekar, and N. Rajini, "Characterization of natural fiber and composites- a review," *Journal of Reinforced Plastics and Composites*, vol. 32, no. 19, pp. 1457–1476, 2013.

[24] G. Raj Kumar, R. Vijayanandh, M. Senthil Kumar, and S. Sathish kumar, "Experimental testing and numerical simulation on natural composite for aerospace applications," *AIP Conference Proceedings*, vol. 1953, 2018.

[25] J. E. Raja Dhas, K. A. Savio Lewise, K. N. Kumar et al., "Effect of coconut shell nanopowder reinforcement in the development of palm fiber composites," *Front. Mater.*, vol. 9, Article ID 986011, 2022.

[26] J. Edwin Raja Dhas, K. Anton Savio Lewise, N. Kumar Kulandaiyappan et al., "Manufacturing and experimental characterization of new-developed natural fiber reinforced polymer Nanocomposite," *Journal of Materials Research and Technology*, vol. 26, pp. 6084–6095, 2023.

[27] Y. Wang, V. Raja, S. K. Madasamy et al., "Multi-parametric investigations on aerodynamic force, aeroacoustic, and engine energy utilizations based development of intercity bus associates with various drag reduction techniques through advanced engineering approaches," *Sustainability*, vol. 14, no. 10, p. 5948, 2022.

[28] Y. Jiang, A. P. Raji, V. Raja et al., "Multi–disciplinary optimizations of small-scale gravitational vortex hydropower (SGVHP) system through computational hydrodynamic and hydro–structural analyses," *Sustainability*, vol. 14, no. 2, p. 727, 2022.

[29] R. Vijayanandh, M. Senthil Kumar, K. Naveenkumar, G. Raj Kumar, and R. Naveen Kumar, "Design optimization of advanced multi-rotor unmanned aircraft system using FSI," *Lecture Notes in Mechanical Engineering*, vol. 2, pp. 299–310, 2018.

[30] R. A. Prakash, R. Vijayanandh, K. N. Kumar et al., "Structural optimization for gravitational vortex hydropower's rotor through hydro-structural interaction [HSI] analysis," *AIP Conference Proceedings*, vol. 2446, Article ID 180022, 2022.